



1 **Biological data assimilation for parameter estimation of a**  
2 **phytoplankton functional type model for the western North Pacific**

3

4 \*Yasuhiro Hoshihara<sup>1,2</sup>, Takafumi Hirata<sup>1</sup>, Masahito Shigemitsu<sup>3</sup>, Hideyuki Nakano<sup>4</sup>, Taketo Hashioka<sup>3</sup>,  
5 Yoshio Masuda<sup>1</sup>, Yasuhiro Yamanaka<sup>1</sup>

6 <sup>1</sup>Faculty of Environmental Earth Science, Hokkaido University, Japan

7 <sup>2</sup>Atmosphere and Ocean Research Institute, The University of Tokyo, Japan

8 <sup>3</sup>Japan Agency for Marine-Earth Science and Technology

9 <sup>4</sup>Meteorological Research Institute, Japan Meteorological Agency

10 *Correspondence to:* Yasuhiro Hoshihara (hoshi-y@aori.u-tokyo.ac.jp)

11 **Abstract.** Ecosystem models are used to understand ecosystem dynamics and ocean biogeochemical cycles and require  
12 optimum physiological parameters to best represent biological behaviours. These physiological parameters are often tuned  
13 up empirically, while ecosystem models have evolved to increase the number of physiological parameters. We developed a  
14 three-dimensional (3D) lower trophic level marine ecosystem model known as the Nitrogen, Silicon and Iron regulated  
15 Marine Ecosystem Model (NSI-MEM) and employed biological data assimilation using a micro-genetic algorithm to  
16 estimate 23 physiological parameters for two phytoplankton functional types in the western North Pacific. The approach  
17 used a one-dimensional emulator that referenced satellite data. The 3D NSI-MEM with biological parameters optimised by  
18 assimilation improved the timing of a modelled plankton bloom in the subarctic and subtropical regions compared to models  
19 without data assimilation. Furthermore, the model was able to simulate not only surface concentrations of phytoplankton but  
20 also subsurface maximum concentrations of phytoplankton. Our results show that surface data assimilation of biological  
21 parameters from two observatory stations benefits the representation of vertical plankton distribution in the western North  
22 Pacific.

23



## 24 1 Introduction

25 Processes of growth, decay and interaction by plankton in the lower trophic level (LTL) marine ecosystem are critical to  
26 understand the oceanic biogeochemical cycles. There are many LTL marine ecosystem models ranging from simple nutrient,  
27 phytoplankton and zooplankton models to more complicated models including carbon-, oxygen-, silicate-, iron-cycles and so  
28 forth (e.g. Edwards and Brindley, 1996; Fasham et al., 1990; Shigemitsu et al., 2012; Yamanaka et al., 2004; Yoshikawa et al.,  
29 2005). Coupling LTL marine ecosystem models to ocean general circulation models (OGCMs) makes it possible to discuss  
30 the three-dimensional (3D) quantitative descriptions of the ecosystem and to investigate temporally fine variability (e.g. Aita  
31 et al., 2007; Hashioka et al., 2009; Hoshiba and Yamanaka, 2016; Masuda et al., 2017; Sumata et al., 2010). Physiological  
32 parameters are usually fixed on the basis of local estimations and applied homogeneously to a basin-scaled ocean, although  
33 the values of physiological parameters should depend on the environments of regions. Physiological parameters have often  
34 been tuned up empirically and arbitrarily, although ecosystem models have recently added more parameters to increase the  
35 number of prognostic and diagnostic variables. A reasonable estimate of the physiological parameters in ecosystem models  
36 is required to reproduce the observed data such as the spatial distribution patterns of phytoplankton biomass and the timing  
37 of a plankton bloom.

38 In previous studies using LTL marine ecosystem models, various approaches for data assimilation were introduced as  
39 methods of estimating optimal physiological parameters (e.g. Kuroda and Kishi, 2004; Fiechter et al., 2013; Toyoda et al.,  
40 2013; Xiao and Friedrichs, 2014). In this study, to estimate the optimal parameter sets, we employed a data assimilative  
41 approach by using a micro-genetic algorithm ( $\mu$ -GA) (Krishnakumar, 1990) with a LTL marine ecosystem model: the  
42 nitrogen, silicon and iron regulated marine ecosystem model (NSI-MEM) (Shigemitsu et al., 2012). This algorithm had  
43 already been adopted and confirmed to work well in the one-dimensional (1D) NSI-MEM of the western subarctic Pacific by  
44 Shigemitsu et al. (2012). Shigemitsu et al. (2012) had developed the NSI-MEM based on NEMURO (North Pacific  
45 Ecosystem Model for Understanding Regional Oceanography: Kishi et al., 2007) the following points: (1) the introduction of  
46 an iron cycle, including dissolved and particulate iron, whereby the dissolved iron explicitly regulates  
47 phytoplankton-photosynthesis; (2) adoption of physiologically more consistent optimal nutrient-uptake (OU) kinetics  
48 compared to the classical Michaelis–Menten equation and (3) the division of detritus into two types of small and large sizes  
49 that exhibit different sinking rates among other things.

50 We used the 3D NSI-MEM and the Parameter-optimised approach for the phytoplankton components to improve the  
51 model's performance in terms of biomass and seasonal fluctuations of phytoplankton in the western North Pacific (WNP)  
52 region. In the WNP region, there are both subarctic and subtropical gyres comprising the Oyashio and the Kuroshio,  
53 respectively. Between the gyres (i.e. the Kuroshio–Oyashio transition region), horizontal gradients of temperature and  
54 phytoplankton concentration in the surface water are generally large due to meanders in the Kuroshio extension jet and  
55 mesoscale eddy activity (Qiu and Chen, 2010; Itoh et al., 2015). The WNP region is a high-nutrient, low-chlorophyll



56 (HNLC) region where biological productivity is lower than expected for the prevailing surface macronutrient conditions. The  
57 relatively low productivity in the HNLC region is due to low dissolved iron concentrations (e.g. Tsuda et al., 2003), because  
58 iron is one of the essential micronutrients for many phytoplankton species. The source of iron for the WNP region is not only  
59 from air-born dust but also from iron transported in the intermediate water from the Sea of Okhotsk to the Oyashio region  
60 (Nishioka et al., 2011). Since the WNP region exhibits many complex physical and biogeochemical characteristics as  
61 referred to above, it is difficult even for state-of-the-art eddy-resolving models to reproduce them. As a trial toward better  
62 simulating the LTL ecosystem in the WNP region, we introduced the following into the NSI-MEM: (1) a data assimilated  
63 physical field by eddy-resolving OGCM with a horizontal resolution of  $0.1^\circ$  and (2) an assimilated physiological parameter  
64 estimation for two different phytoplankton groups. We also focused on the seasonal variations of phytoplankton.  
65

## 66 **2 Model and data description**

### 67 **2.1 Setting the 3D NSI-MEM**

68 We used the marine ecosystem model, 3D NSI-MEM, and included two phytoplankton functional types (PFTs): non diatom  
69 small phytoplankton (PS) and large phytoplankton like diatoms (PL) (Fig. 1). We also used a physical field obtained from  
70 the Meteorological Research Institute Multivariate Ocean Variational Estimation for the WNP region (MOVE-WNP) (Usui  
71 et al., 2006). The MOVE-WNP system is composed of an OGCM and a multivariate 3D variational analysis scheme that  
72 synthesizes the observed information such as temperature, salinity and sea surface height.

73 The model domain extends from  $15^\circ$  N to  $65^\circ$  N and  $117^\circ$  E to  $160^\circ$  W, with a grid spacing of  $1/10^\circ \times 1/10^\circ$  around Japan  
74 and  $1/6^\circ$  to the north of  $50^\circ$  N and to the east of  $160^\circ$  E (Fig. 2 (a)). There are 54 vertical levels with layer thicknesses  
75 increasing from 1 m at the surface to 600 m at the bottom. The model is forced by factors including surface wind, heat flux  
76 and freshwater flux. The details of the surface forcing are presented by Tsujino et al. (2011). Dust flux for dissolved iron and  
77 short wave radiation input were similar to that of a global climate model (Model for Interdisciplinary Research on Climate;  
78 Watanabe et al., 2011), and river run-off as a nutrient supply was from CORE ver. 2 forcing (Large and Yeager, 2009).  
79 Nutrients near the boundary were restored to the values provided by a model, Marine Ecosystem Model CCSR Ocean  
80 Component Model (MEM-COCO), participating in MARine Ecosystem Model Intercomparison Project. The physical field  
81 used in our ecosystem model had already been confirmed to reproduce realistic salinity, velocity and temperature fields in a  
82 previous study (Usui et al., 2006). Using a physical one-day averaged field, we ran the NSI-MEM to simulate the years  
83 between 1985 and 1998. The results from 1998 were analysed in this study.

84 We divided the model domain into two provinces (green and yellow regions in Fig. 2 (b)) using the following province map  
85 instead of maps divided by latitude–longitude lines as in previous studies (e.g. Longhurst, 1995; Toyoda *et al.*, 2013). The  
86 province map is based on the dominant phytoplankton species and nutrient limitations (Hashioka et al., in preparation) and  
87 sets different ecosystem parameters (see details in Sect. 2.3) for each province (hereafter, ‘Parameter-optimised case’; Table



88 1). The respective parameters for each province were estimated by the 1D NSI-MEM using the  $\mu$ -GA employed by those  
 89 in the 3D model. We also conducted model simulations with the similar parameters, as a parameter set for the whole  
 90 domain, to Shigemitsu et al. (2012) (hereafter ‘Default case’, Table 1). In order to smooth the gap in parameter values at the  
 91 boundary between the two provinces in Fig. 2 (b), the parameters were varied as a function of the sea surface temperature  
 92 (SST) annually averaged for 1998 (Fig. 2 (c)) for our ‘SST-dependent case’ (Table 1). The parameters were  
 93 interpolated/extrapolated according to the following equation:

$$94 \quad P(x) = P_{St.S1} + (P_{St.KNOT} - P_{St.S1}) \times \frac{SST(x) - SST_{St.S1}}{SST_{St.KNOT} - SST_{St.S1}}, \quad (1)$$

95 where  $P(x)$ ,  $P_{St.S1}$  and  $P_{St.KNOT}$  are ecosystem parameters for a point  $(x)$ , St. S1 and St. KNOT, respectively. St. KNOT and  
 96 St. S1 are typical observational points in the subarctic and subtropical regions (green- and yellow-coloured areas in Fig. 2 (b),  
 97 respectively). The parameters of all the 3D experimental cases, shown in Table 1, were not changed either vertically or  
 98 temporally.

## 99 2.2 Satellite and in situ data

100 Global satellite data for 1998 for phytoplankton (i.e. chlorophyll a) were obtained from the Ocean Colour Climate Change  
 101 Initiative dataset, European Space Agency, available online at <http://www.esa-oceancolour-cci.org/>, which utilises the data  
 102 archives of ESAs MERIS/ENVISAT and NASAs SeaWiFS/SeaStar, Aqua/MODIS. The global satellite data were linearly  
 103 interpolated to the grid (size  $1/10^\circ$  and  $1/6^\circ$ ) in the model domain (Fig. 2 (a)), and the nitrogen-converted concentrations of  
 104 both PL and PS were estimated by a satellite PFT algorithm (Hirata et al., 2011). The  $\mu$ -GA cost function was defined from  
 105 the 1998 monthly averaged PL and PS concentrations. Satellite data of the 1998 mean SST from the AVHRR Pathfinder  
 106 Project (<http://www.nodc.noaa.gov/SatelliteData/pathfinder4km/>) were also used to conduct our SST-dependent case study  
 107 using the same interpolation as above.

108 To validate the vertical distribution of the model results, we utilised in situ data of phytoplankton and nutrients at St. KNOT  
 109 ( $44^\circ$  N,  $155^\circ$  E) obtained from the web site (<http://www.mirc.jha.or.jp/CREST/KNOT/>) (Tsurushima et al., 2002).

## 110 2.3 1D NSI-MEM process

111 The 1D NSI-MEM used in Shigemitsu et al. (2012) was employed as an emulator to determine the optimal set of ecosystem  
 112 parameters at St. KNOT ( $44^\circ$  N,  $155^\circ$  E) and S1 ( $30^\circ$  N,  $145^\circ$  E), respectively. We modified the 1D NSI-MEM of Shigemitsu  
 113 et al. (2012) by increasing the number of vertical layers to 54 and introducing the vertical advection of the 3D simulation.  
 114 Twenty-three parameters in the NSI-MEM were selected, as shown in Table 2, which were responsible for PL and PS  
 115 biomass relevant to the photosynthesis and grazing of zooplanktons. The other parameters were similar to those in the  
 116 Default case. The initial (1<sup>st</sup> January 1998) and boundary conditions during the integration period were applied from those in  
 117 the 3D model.



## 118 2.4 $\mu$ -GA implementation

119 The  $\mu$ -GA procedure included the following: (1) a cost function was defined; (2) higher evaluated model results of  
 120 parameter information were maintained (following Step 2 to 5) and (3) optimized parameter set was estimated through  
 121 repeating the process of (2) multiple times (following Step 6). To define the cost function, satellite PFT data were used as  
 122 reference values for the  $\mu$ -GA because satellite data have higher temporal and spatial resolution than in situ data.

123 Running the 1D NSI-MEM with the  $\mu$ -GA, 23 optimal parameters were obtained through the following process:

124 **Step 0** Define a range of parameter values (Table 2) based on previous studies (e.g. Jiang et al., 2003; Fujii et al., 2005;  
 125 Yoshie et al., 2007) and prepare 23 population size being the same number of estimated parameters before running the  $\mu$ -GA.

126 **Step 1** Generate 23 initial random parameter strings using the  $\mu$ -GA.

127 **Step 2** Evaluate the 23 model runs with the different parameter strings using the following cost function:

$$128 \quad Cost = \sum_i \frac{1}{N_i} \sum_j^M \frac{1}{\sigma_i^2} (m_{ij} - d_{ij})^2, \quad (2)$$

129 where  $m_i$  is the modelled monthly mean of phytoplankton type  $i$  ( $i = 1$  for PL and 2 for PS) and  $d_i$  is the monthly satellite  
 130 data of the type  $i$ . The index  $j$  denotes the number of months ( $N_j$ ) for which satellite data of type  $i$  exists. The assigned  
 131 weights for PL and PS are  $\sigma_{PL} = 0.1 \mu\text{mol/l}$  and  $\sigma_{PS} = 0.1 \mu\text{mol/l}$ .

132 **Step 3** Determine the best parameter string and carry it forward to the next model run (or the next ‘generation’) (elitist  
 133 strategy).

134 **Step 4** Choose the remaining 22 strings for re-determination of the best parameter strings (or ‘reproduction’) based on a  
 135 deterministic tournament selection strategy (the best string that gave the highest model performance in Step 3 also competes  
 136 for its copy in the reproduction). In the tournament selection strategy, the strings are grouped randomly and adjacent pairs are  
 137 made to compete. Apply crossover to the winning pairs and generate new parameter strings for the final 22 strings. Two  
 138 copies of the same string mating for the next generation should be avoided.

139 **Step 5** If the difference between the maximum and minimum cost function values of the populations becomes too small,  
 140 renew all the parameter strings randomly except for the best-performed string for efficiently escaping from a local solution;  
 141 the cost function may have local minimums.

142 **Step 6** Repeat the procedure from Step 2 to Step 5 until the best parameter strings are un-changed (i.e. parameters are  
 143 well converged within 2,000 generations (times) in the present study).

144 The 1D NSI-MEM was used as an emulator to determine ecosystem parameters through the process described above, and  
 145 the parameter sets assimilated by the 1D model with the  $\mu$ -GA at St. KNOT and St. S1 were applied to the 3D simulations  
 146 which were conducted as the Parameter-optimised case and the SST-dependent case in Table 1.

## 147 3. Results and discussion



### 148 3.1 1D model

149 The 1D NSI-MEM was employed as an emulator to determine ecosystem parameters. Seasonal variations in the Default  
150 and Parameter-optimised cases simulated those from the satellite data as follows: the PS biomass was larger than the PL  
151 biomass at both St. KNOT and St. S1, but the relative ratio of PL to the total biomass at St. KNOT was larger than that at St.  
152 S1 (Fig. 3). These results are consistent with the general understanding that the subarctic region biomass is larger than the  
153 subtropical region biomass. Moreover, diatoms, represented as PL, are a major group in the subarctic region.

154 The seasonal variations of PS in the Parameter-optimised case (dashed lines) for the two stations simulated by the satellite  
155 data (solid lines) were more accurate than those in the Default case (dotted lines). There were small seasonal variations with  
156 a winter peak of 0.6–0.7 molN/m<sup>3</sup> at St. KNOT, and a relatively large seasonal variation with a spring peak of 0.65 molN/m<sup>3</sup>  
157 at St. S1 except double the biomass observed by the satellite (0.33 molN/m<sup>3</sup>). For PL, the seasonal peaks in winter at St.  
158 KNOT (0.57 molN/m<sup>3</sup>) and in spring at St. S1 (0.08 molN/m<sup>3</sup>) in the Parameter-optimised case captured those in the satellite  
159 data independent of the large differences in biomass.

### 160 3.2 3D model

161 The parameter sets assimilated by the 1D model at St. KNOT and St. S1 were applied to the 3D simulation. The seasonal  
162 variation features in the 3D simulation were similar to those seen in the 1D simulation (i.e. relatively small seasonal  
163 variations of PS biomass in the subarctic region and relatively high winter biomass in the Parameter-optimised case  
164 compared to the Default case). The PL biomass features were similar to those of the PS biomass, mentioned above, except  
165 that the PL biomass was lower in the subtropical region in the Parameter-optimised case than in the Default case. Seasonal  
166 peaks of PS and PL biomass also had the same features as those in the 1D simulations (i.e. the PS bloom in the  
167 Parameter-optimised case occurred from winter to spring (Fig. 4 (c), (g)), but that in the Default case occurred in summer  
168 (Fig. 4 (b)).

169 Higher phytoplankton concentrations were found in coastal areas throughout the year in the satellite data. The model could  
170 not simulate these high concentrations. This may be due to the inaccuracy of the satellite data resulting from the high  
171 concentrations of dissolved organic material and inorganic suspended matter (e.g. sand, silt and clay), and/or due to the  
172 uncertainty in the model introduced by unaccounted coastal dynamics such as small-scale mixing processes.

### 173 3.3 Amplitude and phase of seasonal phytoplankton fluctuations

174 At the St. KNOT and St. S1 stations, seasonal variation in total phytoplankton concentrations in the Parameter-optimised  
175 case were better reproduced to those in the satellite data than those in the Default case (Fig. 5). At St. KNOT (Fig. 5 (a)), the  
176 phytoplankton bloom in the Parameter-optimised case occurs in winter, and the phytoplankton bloom in the Default case  
177 occurs in summer with an anti-phase to that of the satellite. At St. S1 (Fig. 5 (b)), the timing of maximum phytoplankton  
178 concentration in the Parameter-optimised case matches that of the satellite regardless of its larger seasonal variation  
179 amplitude compared to those in the satellite and the Default cases. The seasonal variations for each of the PS and PL



180 concentrations are similar to the total phytoplankton concentrations (not shown) compared with the two model cases.

181 Figure 6 shows the amplitude and the phase of seasonal variations in the three model cases (Default, Parameter-optimised  
182 and SST-dependent) compared with those from the satellite. Based on the seasonal variation from the satellite, the radius  
183 shows the relative amplitude of seasonal variation for each of the modelled cases, and the angle from the x-axis shows the  
184 maximum concentration time lag for each of the model cases (i.e. the point (1, 0) shown as 'True' is a perfect match to the  
185 satellite data). At St. KNOT, the point of the Parameter-optimised case (blue solid vector) was the closest to the satellite data  
186 for all the three modelled cases. The ratios of the amplitudes to the satellite data were as follows: 1.00 for the  
187 Parameter-optimised case (blue solid vector); 1.08 for the SST-dependent case (yellow solid vector) and 1.24 for the Default  
188 case (orange solid vector). The timings of the maximum concentration were as follows: a two-month delay for the  
189 Parameter-optimised case (blue solid vector); a three-month delay for the SST-dependent case and a six month delay  
190 (anti-phase) for the Default case. The timing of the Parameter-optimised case at St. S1 (blue broken vector) was improved,  
191 though its seasonal amplitude was not improved.

192 Optimisation of the physiological parameters by assimilating them to the satellite data at the two stations improved the  
193 seasonal variations of the phytoplankton concentrations such as the timing of the bloom and the seasonal amplitude of the  
194 WNP region.

### 195 3.4 Comparison with vertical distributions

196 The model-simulated vertical distributions of phytoplankton and nitrate concentrations from St. KNOT on 20<sup>th</sup> July, 1998  
197 were compared with the observed on the same day in situ data (Fig. 7). The vertical distribution of phytoplankton in the  
198 Parameter-optimised case was closer to the in situ data compared to the Default case data (Fig. 7 (a)). The maximum  
199 phytoplankton concentration for the Parameter-optimised case and the in situ data were located in the subsurface around a  
200 depth of 50 m, while there was no subsurface maximum in the Default case. This was an interesting improvement because  
201 physiological parameters were optimised using only surface satellite data. Moreover, data assimilation not only improved the  
202 surface concentration but also the important characteristics of vertical plankton distribution such as the subsurface maximum  
203 by changing the physiological parameters.

204 In the NEMURO, the predecessor version of the NSI-MEM, the amplitude and timing of phytoplankton blooms are  
205 predominantly controlled by the photosynthesis rate (i.e. bottom-up effect of nutrient dependence) rather than the grazing  
206 rate (i.e. top-down effect of zooplanktons) (Hashioka et al., 2013). The former was determined by the smallest limited  
207 growth rate of nitrogen ( $\text{NH}_4$  and  $\text{NO}_3$ ), silicate ( $\text{Si}(\text{OH})_4$ ) and dissolved iron (FeD) (refer to Eq. (A15) and Eq. (A23) in  
208 Shigemitsu et al., 2012). For PS and PL in the Parameter-optimised case and Default case, the dissolved-iron-limited growth  
209 rates (yellow lines) dominate the photosynthesis (Fig 8). These increased remarkably in the subsurface layer (below a depth  
210 of 50 m) because of the parameter optimisation of the potential maximum growth rate ( $V_0$ ) and the affinity ( $A_0$ ) as shown in  
211 Table 2.

212 As a result, the uptake of dissolved iron was improved, particularly in the subsurface layer, leading to an increase of the



213 phytoplankton biomass (Fig. 7 (a)). The larger biomass of phytoplankton also consumed more nitrate and silicate nutrients  
214 resulting in a lower nitrate concentration compared to that in the Default case above a depth of 140 m (Fig. 7 (b)).

215 The change in the dissolved-iron-limited growth rates resulted from the lower concentration of dissolved iron in the  
216 subarctic area (Fig. 9) because of the greater consumption of FeD by the phytoplankton compared to that in the Default case.  
217 In the Parameter-optimised case (Fig. 9 (b)), the low concentration of dissolved iron in the subarctic region (north of 40° N)  
218 is consistent with the conception of a HNLC region in the North Pacific Ocean (Moore et al., 2013).

### 219 3.5 Physiological parameter changes with ambient conditions

220 The SST-dependent case (i.e. smoothed changing parameters) was compared to the Parameter-optimised case (i.e.  
221 boundary-gap parameters). The horizontal distribution of the PS and PL concentrations in the SST-dependent case were not  
222 significantly different from those in the Parameter-optimised case (Fig. 4) except in two regions—the western region of low  
223 latitude (15° N to 25° N and 120° E to 150° E during January and April in Fig. 4 (h)), and the region adjacent to the  
224 Kuroshio Extension (around 40° N during July to October in Fig. 4 (h)). The former exception is due to the extrapolation of  
225 parameters with high SST and the latter is due to smoothing of parameters between the St. KNOT and St. S1 stations. The  
226 simulated seasonal variations of phytoplankton concentration in the SST-dependent case are slightly worse than those in the  
227 Parameter-optimised case at the two stations (Fig. 6). However, a smoothed set of parameters dependent on the SST prevents  
228 the artificial gap of the parameter value at the fixed boundary between the two provinces.

229 Physiological parameters in ecosystem models change with the surrounding conditions (e.g. nutrient abundance, light  
230 intensity and SST). Smith and Yamanaka (2007) and Smith et al. (2009) suggested the significance of photo-acclimation and  
231 nutrient affinity acclimation. Phytoplankton cells change their traits (e.g. nutrient channel, enzyme) in response to ambient  
232 nutrient concentrations, and typically large (small) cells adapt to low (high) light and high (low) nutrient concentrations  
233 (Smith et al., 2015). In the NSI-MEM, the effect of nutrient-uptake responses by plankton acclimated to different ambient  
234 nutrient conditions is applied as an OU kinetic formulation, but the effect of photo-acclimation has not yet been introduced.  
235 As a first trial of the 3D NSI-MEM, the effect of the physiological parameter change with time was not included in this study,  
236 due to the difficulties and complexities of the scientific interpretation (Schartau et al., 2016). However, the effects of  
237 seasonal variation on the physiological parameters seems significant; thus, the variation effects will be added to the data  
238 assimilation process.

## 239 4 Conclusions

240 We extended a LTL marine ecosystem model, NSI-MEM, into a 3D coupled OGCM. We also used a data assimilation  
241 approach with a  $\mu$ -GA for two different PFTs in the WNP region: non-diatom PS and PL. Twenty-three parameters in the  
242 NSI-MEM were estimated using a 1D emulator with a  $\mu$ -GA parameter-optimisation procedure, referred to as satellite data.  
243 By applying the optimised parameters to the 3D NSI-MEM Parameter-optimised case, the model performances were



244 improved in terms of the seasonal variations of phytoplankton biomass, including the timing of the plankton bloom in the  
245 surface layer, compared to those using prior parameter values (Default case). The vertical distribution of phytoplankton such  
246 as in the subsurface maximum layer were also improved due to the easier-to-use of dissolved iron via the parameter changes,  
247 compared to that in the Default case.

248 Physiological parameters in this study were systematically determined by a  $\mu$ -GA within the range of those used by  
249 numerical models in previous studies. It would be confirmed whether the values of the physiological parameters are  
250 consistent with those observed in situ and/or explained why each parameter is set to an estimated value based on the various  
251 processes (e.g. nutrient bottom-up, zooplankton top-down and particle sinking processes in the ecosystem model).

252

#### 253 Acknowledgements

254 This study was supported by Core Research for Evolutional Science and Technology (CREST), Japan Science and  
255 Technology Agency, Grant Number JPMJCR11A5. The first author developed the 3D NSI-MEM and conducted simulations  
256 using this model at Hokkaido University and analysed the results supported by the Center for Earth Surface System  
257 Dynamics, Atmosphere and Ocean Research Institute, The University of Tokyo. The phytoplankton satellite data were  
258 gathered by the Ocean Colour Climate Change Initiative, ESA (European Space Agency). The SST-satellite data was  
259 provided by the National Oceanic and Atmospheric Administration Pathfinder project in GHRSSST (The Group for High  
260 Resolution Sea Surface Temperature) and the US National Oceanographic Data Center.

261



- 262 References  
263  
264 Aita, M.N., Yamanaka, Y. and Kishi, M.J.: Interdecadal variation of the lower trophic ecosystem in the northern Pacific  
265 between 1948 and 2002, in a 3-D implementation of the NEMURO model, *Ecological Modelling*, 202, 81-94, 2007.  
266 Chai, F., Dugdale, R., Peng, T., Wilkerson, F. and Barber, R.: One-dimensional ecosystem model of the equatorial Pacific  
267 upwelling system. Part I: model development and silicon and nitrogen cycle, *Deep Sea Research Part II: Topical*  
268 *Studies in Oceanography*, 49, 2713-2745, 2002.  
269 Coale, K.H., Wang, X., Tanner, S.J. and Johnson, K.S.: Phytoplankton growth and biological response to iron and zinc  
270 addition in the Ross Sea and Antarctic Circumpolar Current along 170 W, *Deep Sea Research Part II: Topical*  
271 *Studies in Oceanography*, 50, 635-653, 2003.  
272 Edwards, A.M. and Brindley, J.: Oscillatory behaviour in a three-component plankton population model, *Dynamics and*  
273 *Stability of Systems*, 11, 347-370, 1996.  
274 Eslinger, D.L., Kashiwai, M.B., Kishi, M.J., Megrey, B.A., Ware, D.M. and Werner, F.E.: Final report of the international  
275 workshop to develop a prototype lower trophic level ecosystem model for comparison of different marine  
276 ecosystems in the north Pacific, *PICES Scientific Report*, 15, 1-77, 2000.  
277 Fasham, M., Ducklow, H. and McKelvie, S.: A nitrogen-based model of plankton dynamics in the oceanic mixed layer,  
278 *Journal of Marine Research*, 48, 591-639, 1990.  
279 Fiechter, J., Herbei, R., Leeds, W., Brown, J., Milliff, R., Wikle, C., Moore, A. and Powell, T.: A Bayesian parameter  
280 estimation method applied to a marine ecosystem model for the coastal Gulf of Alaska, *Ecological Modelling*, 258,  
281 122-133, 2013.  
282 Fujii, M., Yoshie, N., Yamanaka, Y. and Chai, F.: Simulated biogeochemical responses to iron enrichments in three high  
283 nutrient, low chlorophyll (HNLC) regions, *Progress in Oceanography*, 64, 307-324, 2005.  
284 Hashioka, T., Sakamoto, T.T. and Yamanaka, Y.: Potential impact of global warming on North Pacific spring blooms  
285 projected by an eddy-permitting 3-D ocean ecosystem model, *Geophysical Research Letters*, 36, 2009.  
286 Hashioka, T., Vogt, M., Yamanaka, Y., Le Quere, C., Buitenhuis, E.T., Aita, M., Alvain, S., Bopp, L., Hirata, T., Lima, I.,  
287 Sailley, S. and Doney, S. C.: Phytoplankton competition during the spring bloom in four plankton functional type  
288 models, *Biogeosciences*, 10, 6833-6850, 2013.  
289 Hirata, T., Hardman-Mountford, N., Brewin, R., Aiken, J., Barlow, R., Suzuki, K., Isada, T., Howell, E., Hashioka, T. and  
290 Noguchi-Aita, M.: Synoptic relationships between surface Chlorophyll-a and diagnostic pigments specific to  
291 phytoplankton functional types, *Biogeosciences*, 8, 311-327, 2011.  
292 Hoshiba, Y. and Yamanaka, Y.: Simulation of the effects of bottom topography on net primary production induced by riverine  
293 input, *Continental Shelf Research*, 117, 20-29, 2016.  
294 Itoh, S., Yasuda, I., Saito, H., Tsuda, A. and Komatsu, K.: Mixed layer depth and chlorophyll a: Profiling float observations  
295 in the Kuroshio-Oyashio Extension region, *Journal of Marine Systems*, 151, 1-14, 2015.



- 296 Jiang, M., Chai, F., Dugdale, R., Wilkerson, F., Peng, T. and Barber, R.: A nitrate and silicate budget in the equatorial Pacific  
297 Ocean: a coupled physical–biological model study, *Deep Sea Research Part II: Topical Studies in Oceanography*, 50,  
298 2971-2996, 2003.
- 299 Kishi, M.J., Kashiwai, M., Ware, D.M., Megrey, B.A., Eslinger, D.L., Werner, F.E., Noguchi-Aita, M., Azumaya, T., Fujii, M.  
300 and Hashimoto, S.: NEMURO—a lower trophic level model for the North Pacific marine ecosystem, *Ecological*  
301 *Modelling*, 202, 12-25, 2007.
- 302 Krishnakumar, K.: Micro-genetic algorithms for stationary and non-stationary function optimization, 1989 Symposium on  
303 Visual Communications, Image Processing, and Intelligent Robotics Systems. International Society for Optics and  
304 Photonics, 289-296, 1990.
- 305 Kudo, I., Noiri, Y., Nishioka, J., Taira, Y., Kiyosawa, H. and Tsuda, A.: Phytoplankton community response to Fe and  
306 temperature gradients in the NE (SERIES) and NW (SEEDS) subarctic Pacific Ocean, *Deep Sea Research Part II:*  
307 *Topical Studies in Oceanography*, 53, 2201-2213, 2006.
- 308 Kuroda, H. and Kishi, M.J.: A data assimilation technique applied to estimate parameters for the NEMURO marine  
309 ecosystem model, *Ecological Modelling*, 172, 69-85, 2004.
- 310 Large, W.G. and Yeager, S.G.: The global climatology of an interannually varying air–sea flux data set, *Climate Dynamics*,  
311 33, 341–364, 2009.
- 312 Longhurst, A.: Seasonal cycles of pelagic production and consumption, *Progress in Oceanography*, 36, 77–167, 1995.
- 313 Masuda, Y., Yamanaka, Y., Hirata, T. and Nakano, H.: Competition and community assemblage dynamics within a  
314 phytoplankton functional group: Simulation using an eddy-resolving model to disentangle deterministic and random  
315 effects, *Ecological Modelling*, 343, 1-14, 2017.
- 316 Moore, C.M., Mills, M.M., Arrigo, K.R., Berman-Frank, I., Bopp, L., Boyd, P.W., Galbraith, E.D., Geider, R.J., Guieu, C.,  
317 Jaccard, S.L., Jickells, T.D., La Roche, J., Lenton, T.M., Mahowald, N.M., Marañón, E., Marinov, I.,  
318 Moore, J.K., Nakatsuka, T., Oschlies, A., Saito, M.A., Thingstad, T. F., Tsuda, A. and Ulloa O.: Processes and  
319 patterns of oceanic nutrient limitation, *Nature Geoscience*, 6, 701-710, 2013.
- 320 Nishioka, J., Ono, T., Saito, H., Sakaoka, K. and Yoshimura, T.: Oceanic iron supply mechanisms which support the spring  
321 diatom bloom in the Oyashio region, western subarctic Pacific, *Journal of Geophysical Research: Oceans*, 116,  
322 2011.
- 323 Price, N., Ahner, B. and Morel, F.: The equatorial Pacific Ocean: Grazer–controlled phytoplankton populations in an  
324 iron - limited ecosystem, *Limnology and Oceanography*, 39, 520-534, 1994.
- 325 Qiu, B. and Chen, S.: Eddy-mean flow interaction in the decadal modulating Kuroshio Extension system, *Deep Sea*  
326 *Research Part II: Topical Studies in Oceanography*, 57, 1098-1110, 2010.



- 327 Schartau, M., Wallhead, P., Hemmings, J., Löptien, U., Kriest, I., Krishna, S., Ward, B.A., Slawig, T. and Oschlies, A.:  
328       Reviews and syntheses: Parameter identification in marine planktonic ecosystem modelling, *Biogeosciences*  
329       Discussions, 1-79, 2016.
- 330 Shigemitsu, M., Okunishi, T., Nishioka, J., Sumata, H., Hashioka, T., Aita, M., Smith, S., Yoshie, N., Okada, N. and  
331       Yamanaka, Y.: Development of a one-dimensional ecosystem model including the iron cycle applied to the Oyashio  
332       region, western subarctic Pacific, *Journal of Geophysical Research: Oceans*, 117, 2012.
- 333 Smith, S.L., Pahlow, M., Merico, A., Acevedo-Trejos, E., Sasai, Y., Yoshikawa, C., Sasaoka, K., Fujiki, T., Matsumoto, K.  
334       and Honda, M.C.: Flexible phytoplankton functional type (FlexPFT) model: size-scaling of traits and optimal  
335       growth, *Journal of Plankton Research*, 38, 977-992, 2016.
- 336 Smith, S.L. and Yamanaka, Y.: Quantitative comparison of photoacclimation models for marine phytoplankton, *Ecological*  
337       Modelling, 201, 547-552, 2007.
- 338 Smith, S.L., Yamanaka, Y., Pahlow, M. and Oschlies, A.: Optimal uptake kinetics: physiological acclimation explains the  
339       pattern of nitrate uptake by phytoplankton in the ocean, *Marine Ecology Progress Series*, 384, 1-12, 2009.
- 340 Sugimoto, R., Kasai, A., Miyajima, T. and Fujita, K.: Modeling phytoplankton production in Ise Bay, Japan: Use of nitrogen  
341       isotopes to identify dissolved inorganic nitrogen sources, *Estuarine, Coastal and Shelf Science*, 86, 450-466, 2010.
- 342 Sumata, H., Hashioka, T., Suzuki, T., Yoshie, N., Okunishi, T., Aita, M.N., Sakamoto, T.T., Ishida, A., Okada, N. and  
343       Yamanaka, Y.: Effect of eddy transport on the nutrient supply into the euphotic zone simulated in an  
344       eddy-permitting ocean ecosystem model, *Journal of Marine Systems*, 83, 67-87, 2010.
- 345 Toyoda, T., Awaji, T., Masuda, S., Sugiura, N., Igarashi, H., Sasaki, Y., Hiyoshi, Y., Ishikawa, Y., Saitoh, S. and Yoon, S.:  
346       Improved state estimations of lower trophic ecosystems in the global ocean based on a Green's function approach,  
347       *Progress in Oceanography*, 119, 90-107, 2013.
- 348 Tsuda, A., Takeda, S., Saito, H., Nishioka, J., Nojiri, Y., Kudo, I., Kiyosawa, H., Shiimoto, A., Imai, K., Ono, T., Shimamoto,  
349       A., Tsumune, D., Yoshimura, T., Aono, T., Hinuma, A., Kinugasa, M., Suzuki, K., Sohrin, Y., Noiri, Y., Tani, H.,  
350       Deguchi, Y., Tsurushima, N., Ogawa, H., Fukami, K., Kuma, K. and Saino, T.: A mesoscale iron enrichment in the  
351       western subarctic Pacific induces a large centric diatom bloom, *Science*, 300, 958-961, 2003.
- 352 Tsujino, H., Hirabara, M., Nakano, H., Yasuda, T., Motoi, T. and Yamanaka, G.: Simulating present climate of the global  
353       ocean-ice system using the Meteorological Research Institute Community Ocean Model (MRI.COM): simulation  
354       characteristics and variability in the Pacific sector, *Journal of Oceanography*, 67, 449-479, 2011.
- 355 Tsurushima, N., Nojiri, Y., Imai, K. and Watanabe, S.: Seasonal variations of carbon dioxide system and nutrients in the  
356       surface mixed layer at station KNOT (44 N, 155 E) in the subarctic western North Pacific, *Deep Sea Research Part*  
357       II: Topical Studies in Oceanography, 49, 5377-5394, 2002.
- 358 Usui, N., Ishizaki, S., Fujii, Y., Tsujino, H., Yasuda, T. and Kamachi, M.: Meteorological Research Institute multivariate  
359       ocean variational estimation (MOVE) system: Some early results, *Advances in Space Research*, 37, 806-822, 2006.



- 360 Watanabe, S., Hajima, T., Sudo, K., Nagashima, T., Takemura, T., Okajima, H., Nozawa, T., Kawase, H., Abe, M., Yokohata,  
361 T., Ise, T., Sato, H., Kato, E., Takata, K., Emori, S. and Kawamiya, M.: MIROC-ESM 2010: model description and  
362 basic results of CMIP5-20c3m experiments, *Geosci. Model Dev.*, 4, 845–872, 2011.
- 363 Xiao, Y. and Friedrichs, M. A. M.: The assimilation of satellite-derived data into a one-dimensional lower trophic level  
364 marine ecosystem model, *Journal of Geophysical Research: Oceans*, 119, 2691–2712, 2014.
- 365 Yamanaka, Y., Yoshie, N., Fujii, M., Aita, M.N. and Kishi, M.J.: An ecosystem model coupled with Nitrogen-Silicon-Carbon  
366 cycles applied to Station A7 in the Northwestern Pacific, *Journal of Oceanography*, 60, 227-241, 2004.
- 367 Yoshie, N., Yamanaka, Y., Rose, K.A., Eslinger, D.L., Ware, D.M. and Kishi, M.J.: Parameter sensitivity study of the  
368 NEMURO lower trophic level marine ecosystem model, *Ecological Modelling*, 202, 26-37, 2007.
- 369 Yoshikawa, C., Yamanaka, Y. and Nakatsuka, T.: An ecosystem model including nitrogen isotopes: perspectives on a study of  
370 the marine nitrogen cycle, *Journal of Oceanography*, 61, 921-942, 2005.
- 371



372 Table

373

374 Table 1. List of experiments

	Experiment name	Content of experiment
1D model experiments	Default	Use the almost same parameters as those in Shigemitsu et al. (2012)
	Parameter-optimised	Optimise the parameters with $\mu$ -GA at St. KNOT and St. S1
3D model experiments	Default	The same as default of 1-D model but applied to 3-D simulation
	Parameter-optimised	The same as Parameter-optimised of 1-D model but applied to 3-D simulation for two provinces of Fig. 2 (b)
	SST-dependent	The same as Parameter-optimised of 3-D simulation with interpolated parameters at St. KNOT and St. S1 with SST, instead of parameters for two provinces

375

376 Table 2. NSI-MEM physiological parameters estimated by the  $\mu$ -GA. Max and Min values  
 377 prescribe the upper and lower bounds of the parameter variations used in the previous  
 378 studies. St. Knot and St. S1 indicate optimal estimated values in the provinces of Fig. 2 (b)  
 379 while Default values are previous parameter values.

	Min	KNOT	S1	Default	Max	Unit	Source of Min and Max range
$V_{0,PS}$	0.1	2.7	0.7	0.6	3.2	/day	Shigemitsu et al. (2012)
$A_{0,NO_3,PS}$	1	454	436	30	512	l/molN · s	Shigemitsu et al. (2012)
$K_{NO_3,PS}$	0.50	1.87	2.92	1.00	3.00	$\mu$ molN/l	Chai et al. (2002), Eslinger et al. (2000)
$K_{NH_4,PS}$	0.05	0.12	0.26	0.10	1.00	$\mu$ molN/l	Chai et al. (2002), Eslinger et al. (2000)
$K_{Fed,PS}$	0.035	0.100	0.060	0.040	0.100	nmol/l	Kudo et al. (2006), Price et al. (1994)
$k_{PS}$	0.0392	0.0693	0.0650	0.0693	0.0693	/degC	Eslinger et al. (2000), Fujii et al. (2005)
$M_{PS0}$	0.01208	0.01208	0.04321	0.05850	0.05878	l/ $\mu$ molN · day	Fujii et al. (2005), Sugimoto et al. (2010)
$V_{0,PL}$	0.1	3.2	1.5	1.2	3.2	/day	Shigemitsu et al. (2012)



$A_{0,NO_3,PL}$	1	437	171	10	512	$l/molN \cdot s$	Shigemitsu et al. (2012)
$K_{NO_3,PL}$	0.50	3.00	2.92	3.00	3.00	$\mu molN/l$	Eslinger et al. (2000), Jiang et al. (2003)
$K_{NH_4,PL}$	0.50	0.50	1.31	0.30	2.30	$\mu molN/l$	Eslinger et al. (2000), Fujii et al. (2005)
$K_{SiL,PL}$	3.0	6.0	4.3	6.0	6.0	$\mu mol/l$	Yoshie et al. (2007)
$K_{Fed,PL}$	0.050	0.050	0.089	0.090	0.200	$nmol/l$	Coale et al. (2003)
$k_{PL}$	0.0392	0.0693	0.0392	0.0693	0.0693	$/degC$	Eslinger et al. (2000), Fujii et al. (2005)
$M_{PLO}$	0.02900	0.03694	0.03496	0.02900	0.05878	$l/\mu molN \cdot day$	Fujii et al. (2005), Yamanaka et al. (2004)
$G_{RmaxS}$	0.30	0.79	0.30	0.31	4.00	$/day$	Yoshie et al. (2007), Yoshikawa et al. (2005)
$PS_{ZS^*}$	0.040	0.364	0.364	0.043	0.364	$\mu molN/l$	Eslinger et al. (2000), Sugimoto et al. (2010)
$G_{RmaxL,PS}$	0.05	0.05	0.05	0.10	0.54	$/day$	Eslinger et al. (2000), Fujii et al. (2005)
$G_{RmaxL,PL}$	0.14	0.25	0.14	0.49	0.54	$/day$	Fujii et al. (2005)
$PS_{ZL^*}$	0.0143	0.0430	0.0430	0.0400	0.0430	$\mu molN/l$	Eslinger et al. (2000), Fujii et al. (2005)
$PL_{ZL^*}$	0.0143	0.0430	0.0184	0.0400	0.0430	$\mu molN/l$	Eslinger et al. (2000), Fujii et al. (2005)
$G_{RmaxP,PL}$	0.10	0.40	0.14	0.20	0.40	$/day$	Eslinger et al. (2000)
$PL_{ZP^*}$	0.0143	0.0430	0.0184	0.0400	0.0430	$\mu molN/l$	Eslinger et al. (2000), Fujii et al. (2005)



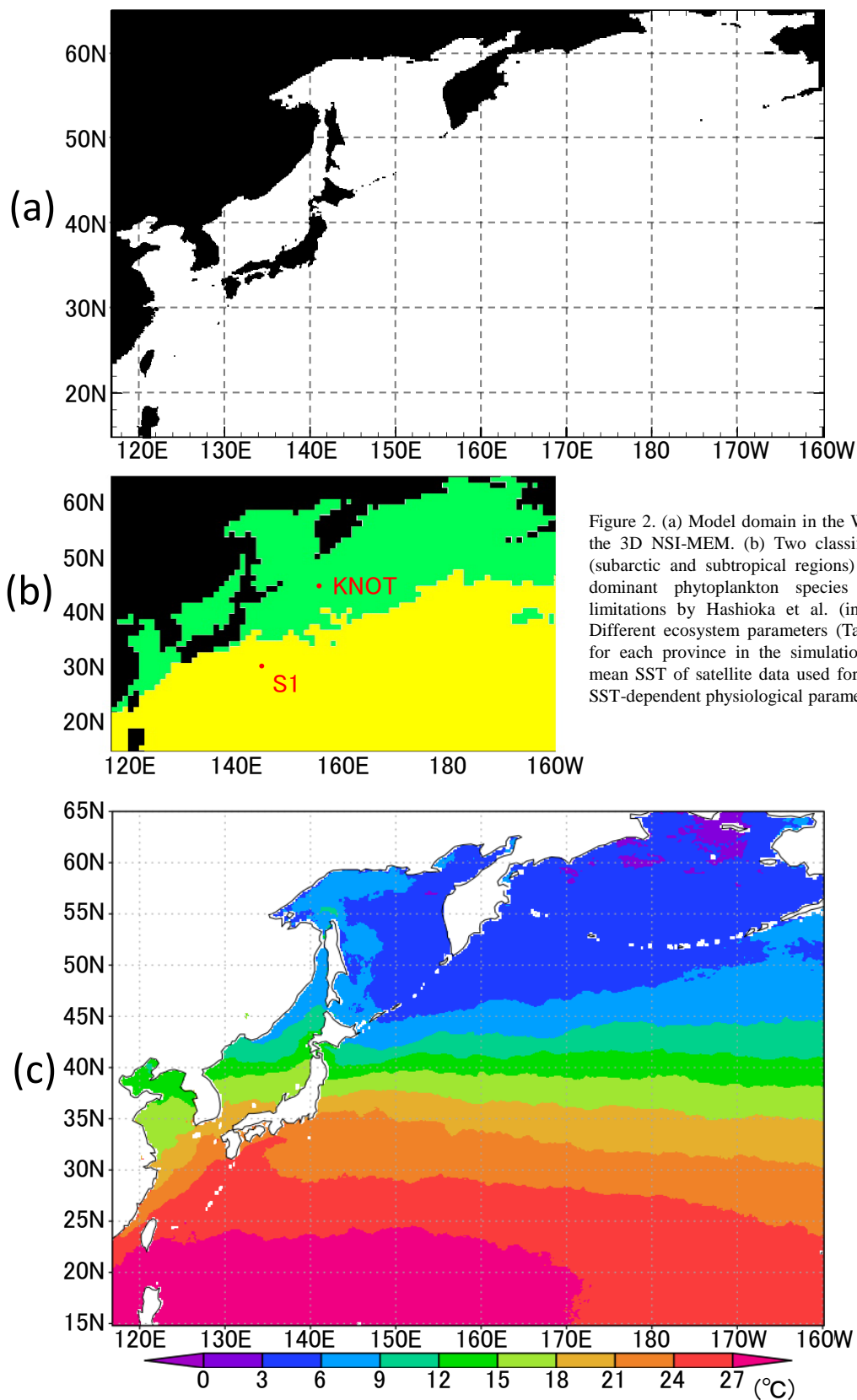
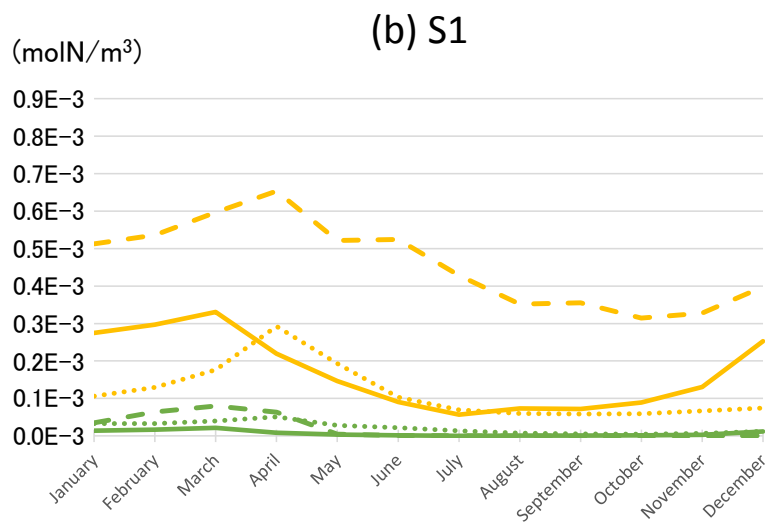
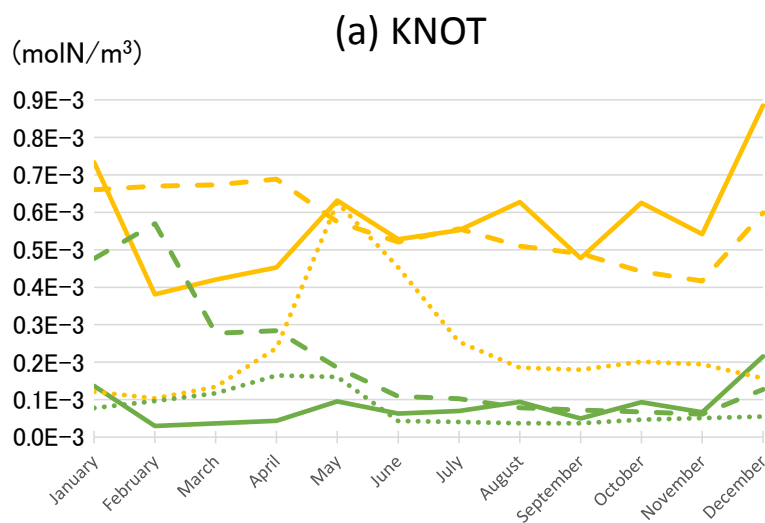


Figure 2. (a) Model domain in the WNP region of the 3D NSI-MEM. (b) Two classified provinces (subarctic and subtropical regions) based on the dominant phytoplankton species and nutrient limitations by Hashioka et al. (in preparation). Different ecosystem parameters (Table 2) are set for each province in the simulation. (c) Annual mean SST of satellite data used for simulation of SST-dependent physiological parameters.



**PS (small phytoplankton)**  
**PL (large phytoplankton)**

— : Satellite data  
 - - - : Parameter-optimised case  
 ..... : Default case

Figure 3. Seasonal variations of surface phytoplankton biomass in the 1D NSI-MEM and satellite data at (a) St. KNOT and (b) St. S1 are shown as typical observational points of the subarctic and the subtropical regions, respectively.

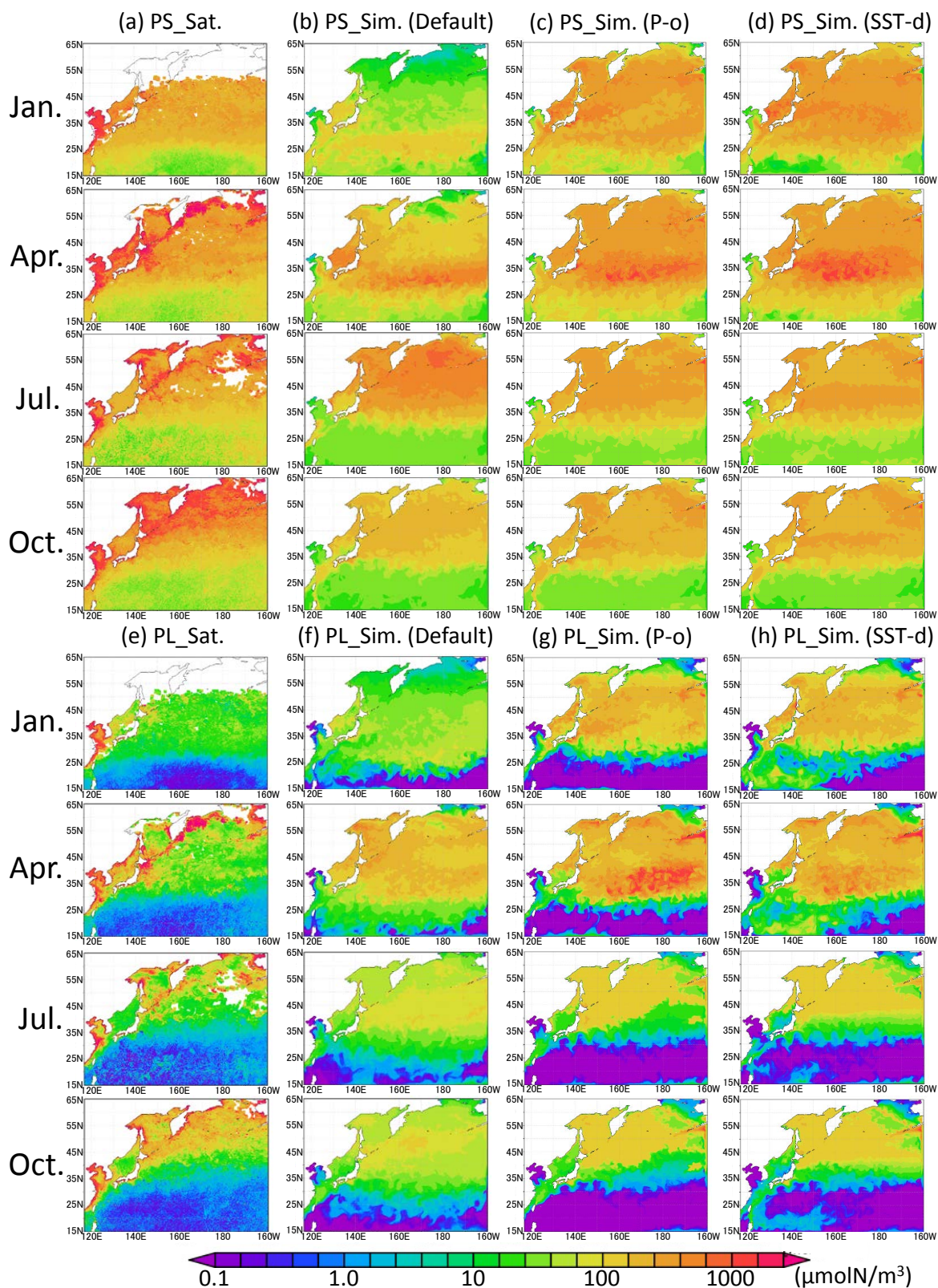


Figure 4. Horizontal distribution of phytoplankton at the surface in 1998. (a) PS (small phytoplankton) from satellites observations, (b) PS in Default case, (c) PS in the Parameter-optimised case, and (d) in the SST-dependent case. (e), (f), (g), (h) are the same except for PL (large phytoplankton). Areas without satellite data are left blank.

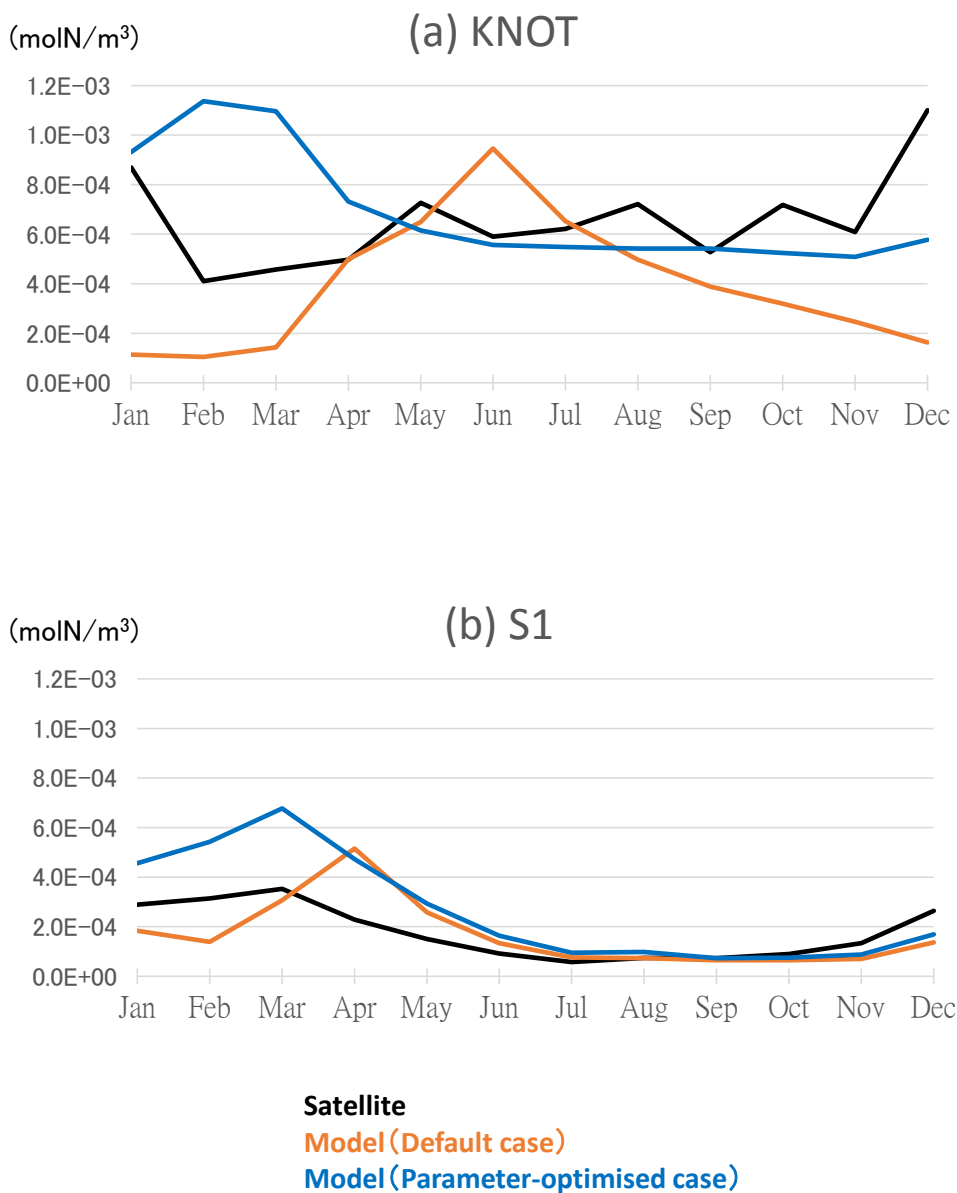


Figure 5. Time series of phytoplankton (PL+PS) concentration in the 3D NSI-MEM and satellite data at (a) St. KNOT and (b) St. S1.

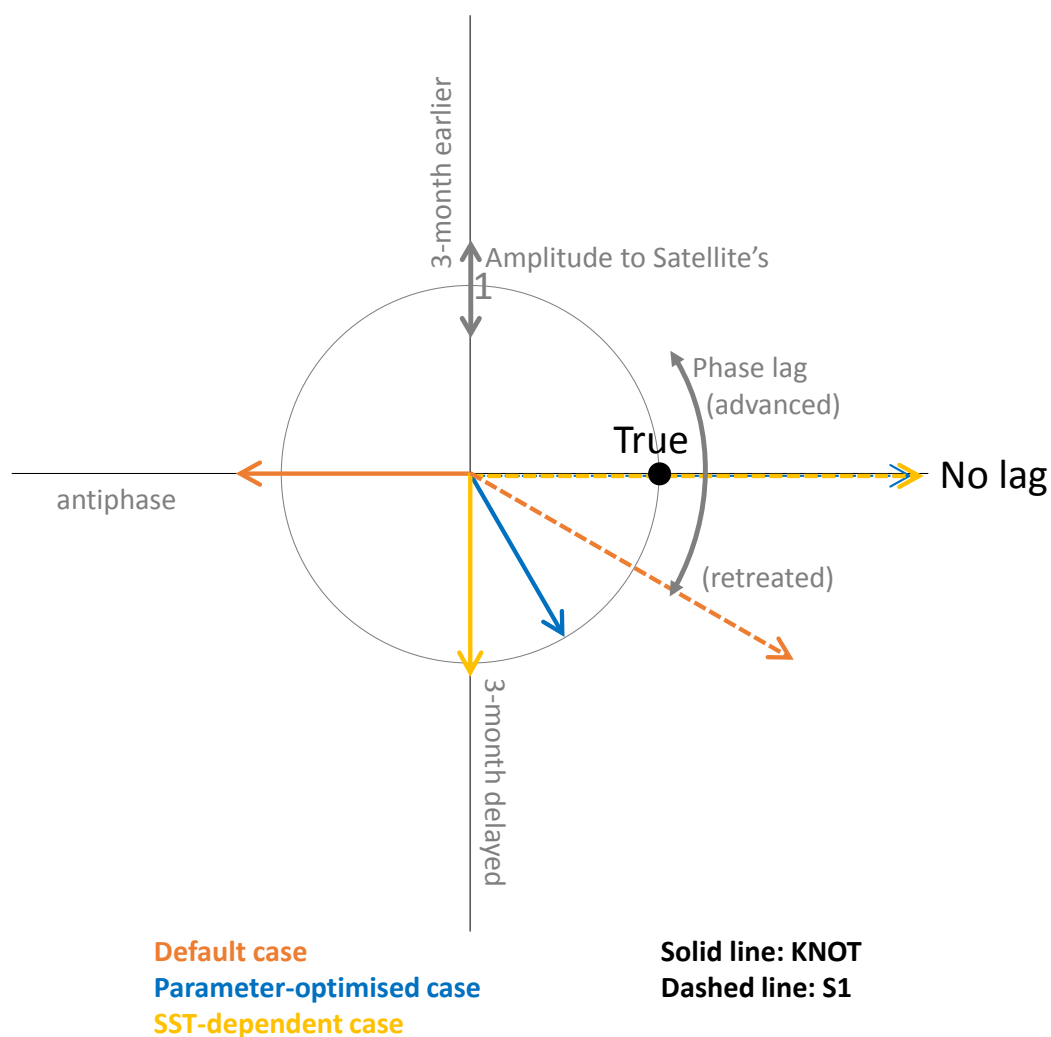


Figure 6. Diagram showing the amplitude and the phase of seasonal variations in the three model cases compared with those in the satellite data. Based on the seasonal variation in the satellite data, the radius indicates the relative amplitude (model/satellite) of seasonal variation for each model case and the angle from the positive x-axis shows the time lag of the maximum concentration for each model case (i.e. the point (1, 0) shown as 'True' is the perfect match to the satellite data). The blue dashed line (Parameter-optimised case at St. S1) and yellow dashed line (SST-dependent case at St. S1) overlap on the no-lagged x-axis.

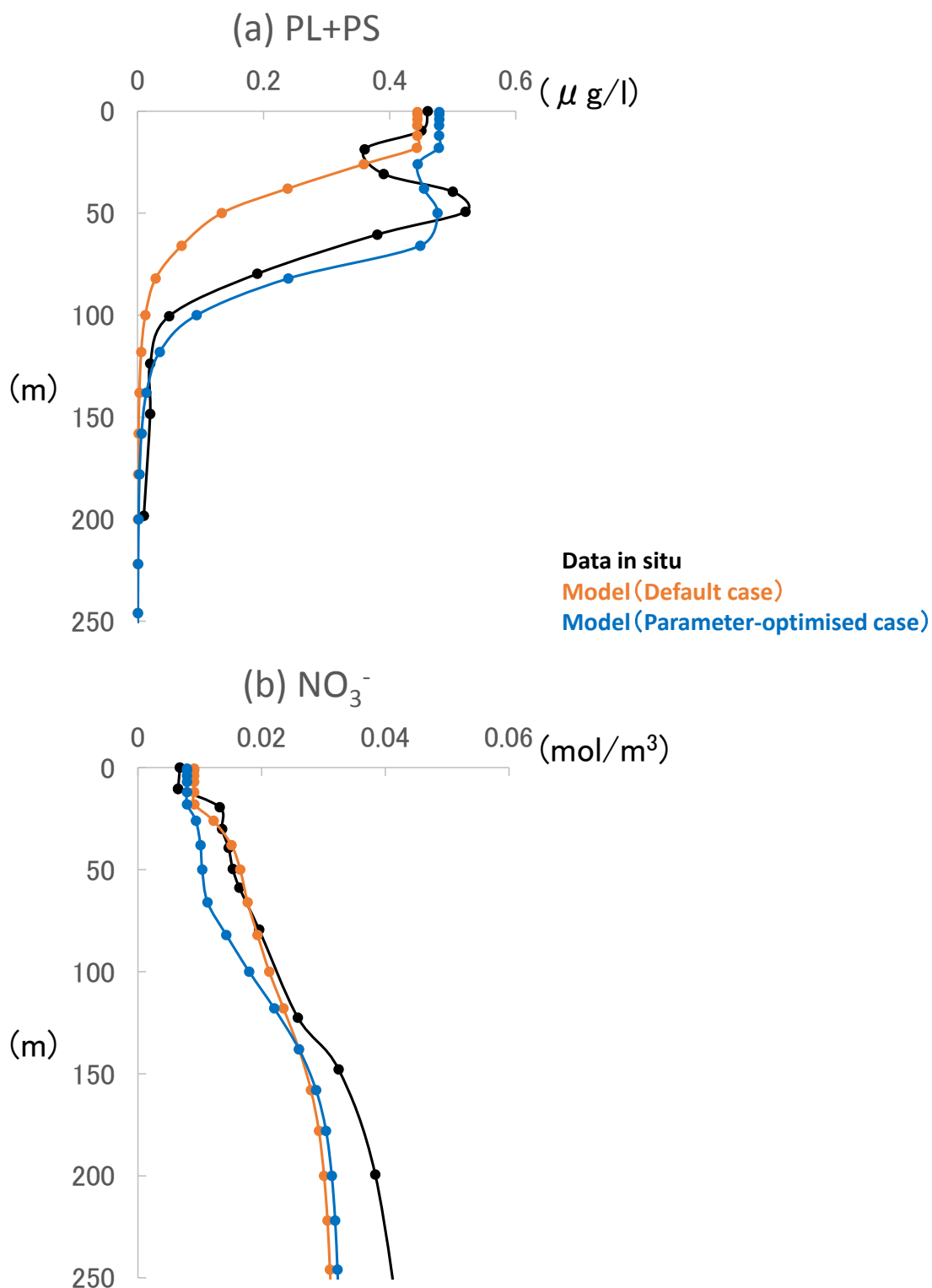
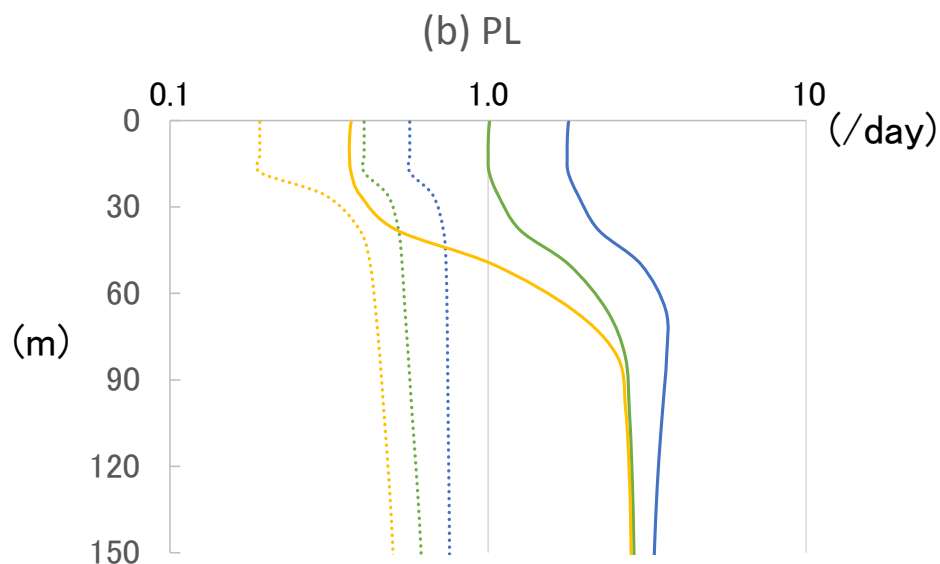
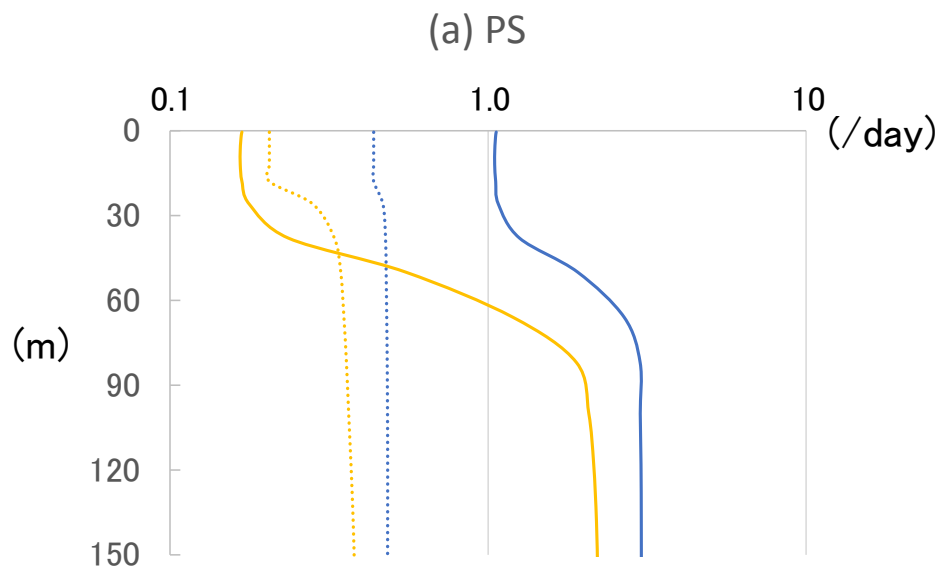


Figure 7. Vertical distributions of (a) phytoplankton (PL+PS) and (b) nitrate concentrations from the 3D model and in situ data at St. KNOT on 20<sup>th</sup> July, 1998.



Limited growth rate by nitrogen  
Limited growth rate by silicate  
Limited growth rate by dissolved iron

Solid line: Parameter-optimised case  
Dotted line: Default case

Figure 8. Vertical distributions of limited growth rates by nitrogen, silicate and dissolved iron simulated from the 3D model of (a) PS and (b) PL at St. KNOT on 20<sup>th</sup> July, 1998.

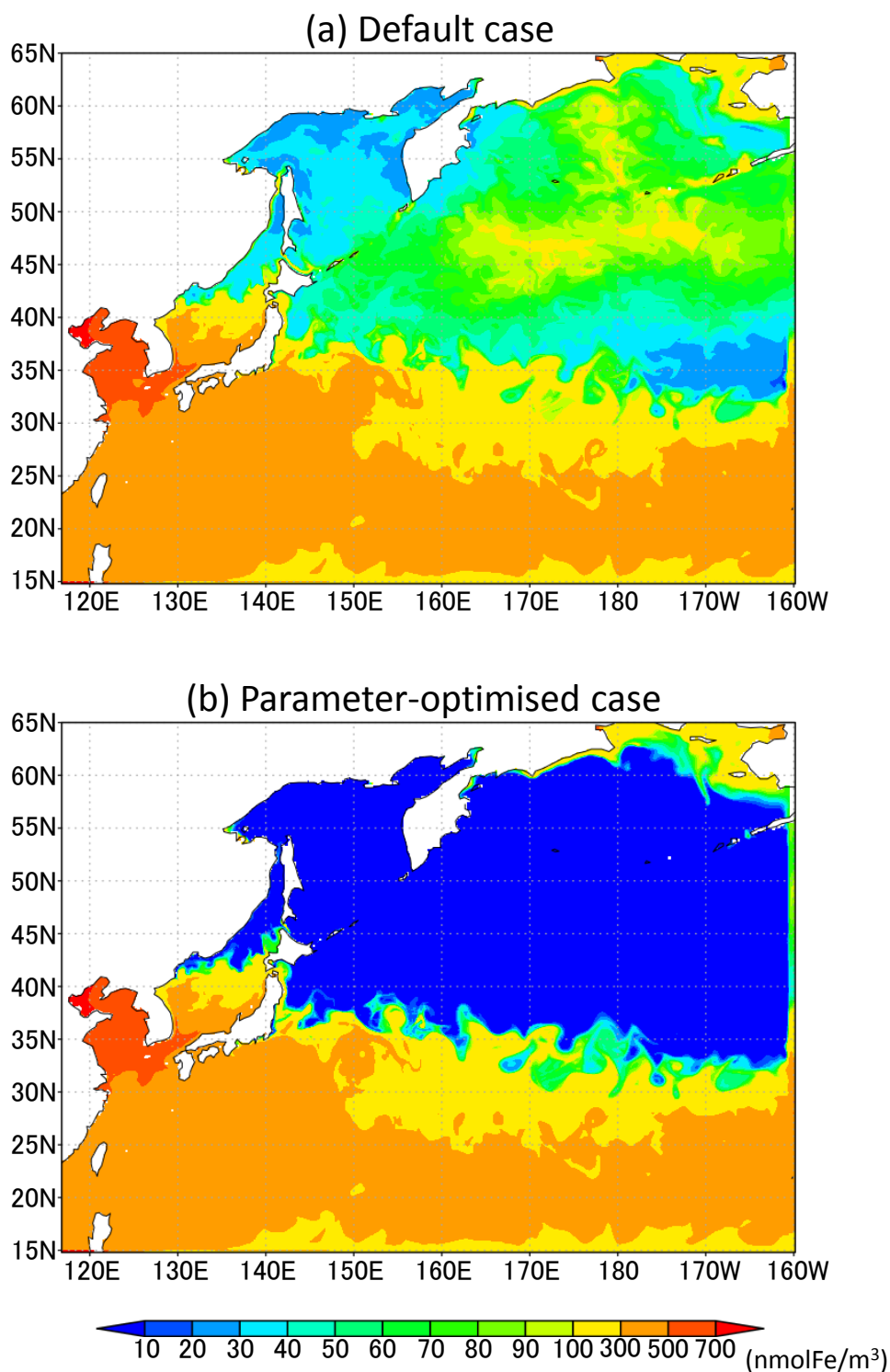


Figure 9. Horizontal distribution of dissolved iron in the surface sea water layer for July 1998; (a) the Default case and (b) the Parameter-optimised case.